IEEE Access
Multidisciplinary | Rapid Review | Open Access Journal

Received 2 December 2023, accepted 7 January 2024, date of publication 17 January 2024, date of current version 30 January 2024.

Digital Object Identifier 10.1109/ACCESS.2024.3355134

RESEARCH ARTICLE

Stability Analysis of a Reconfigurable and Mobile Cable-Driven Parallel Robot

HOR TAN[1], RIZAL MUNTASHIR[2], LATIFAH NURAHMI[3], (Member, IEEE), BAMBANG PRAMUJATI[3], (Member, IEEE), ARI KURNIAWAN[3,4], UNGGUL WASIWITONO[3], (Member, IEEE), AND STÉPHANE CARO[4], (Member, IEEE)

[1]Faculty of Automobile Engineering, National Polytechnic Institute of Cambodia, Phnom Penh 12409, Cambodia
[2]Production Technology Department, Walsin Energy Cable System Company Ltd., Xinzhuang District, New Taipei City 242, Taiwan
[3]Department of Mechanical Engineering, Institut Teknologi Sepuluh Nopember, Surabaya 60111, Indonesia
[4]Department of IT Convergence Engineering, Kumoh National Institute of Technology, Gumi-si, Gyeongsangbuk-do 39177, South Korea

Corresponding author: Bambang Pramujati (pramujati@me.its.ac.id)

This work was supported by the Institut Teknologi Sepuluh Nopember under the Publication Writing and Intellectual property Rights (IPR) Incentive Program (PPHKI) 2024.

ABSTRACT This paper presents a stability analysis based on the Zero Moment Point (ZMP) concept during the reconfiguration of a Cable-Driven Parallel Robot (CDPR) using three mobile bases. Each mobile base can be driven forward and backward, and it has a crane that can be moved up and down, to which a cable connected to the end effector is attached. The ZMP should stay within the designated support boundaries to prevent the robot from tumbling. Therefore, the next positions of the cable exit point are changed by applying two reconfiguration schemes to the robot: 1) changing the mobile base position and 2) altering the crane length. Kinetostatic models of both reconfiguration schemes are formulated such that the wrench matrix is expressed to compute the cable tensions. A fifth-degree polynomial test trajectory is defined to be followed by the end-effector. When executing a prescribed trajectory, the sequence of the mobile base position and the crane length are optimized by continuously considering the robot stability based on ZMP. Without reconfiguration, the mobile cranes cannot handle high cable tensions without tipping over. By performing two reconfiguration schemes, the whole system can be constantly maintained in equilibrium, and the robot's workspace can be enlarged; therefore, the tipping over can eventually be avoided. An experimental setup is built to demonstrate and validate the mathematical models of both reconfiguration scenarios.

INDEX TERMS Cable-driven parallel robot, stability, reconfiguration, crane mechanism, mobile robot, technology.

I. INTRODUCTION

Many researchers are interested in Cable-Driven Parallel Robots (CDPR) due to their large workspace, heavy payload capacity, and high velocity. CDPR has been employed in several applications in the industrial field, and some prototypes have been fabricated, for example, IPAnema [1], and COGIRO [2], [3]. Inverse kinematics, static equilibrium, dynamics, stiffness, and the workspace of CDPR were investigated in [4] and [5]. Interval analysis and cable interference were taken into account in [6] to synthesize the workspace of cable-driven leg training in a gait training machine. The workspace boundaries, leading to the definition of wrench-closure workspace, are numerically determined in [7] which allows the designers to decide whether a pose is acceptable. Wrench-Feasible-Workspace (WFW) is defined as the set of mobile platform poses where the cables can compensate any wrench; therefore, each cable tension remains within a designated tension range [8], [9]. The methodology to trace the WFW based on Available-Wrench-Set (AWS) for mobile CDPR was proposed in [10] and [11]. Two approaches, the convex hull and the hyperplane shifting methods, were introduced to determine the AWS. These approaches were tested for a suspended CDPR performing three-degree-of-freedom (3-DOF) motion to obtain a large workspace. The workspace of tendon-based Stewart

The associate editor coordinating the review of this manuscript and approving it for publication was Xueqin Jiang.

platforms was analyzed in [12]. In [13], the distribution of cable tensions was shown for several trajectories of the end-effector, for example, horizontal or spherical trajectories. The cable tension remains positive and continuous at all times. The S-curve trajectory planning method, which was evaluated for polynomial and trigonometric models, was introduced and formulated in [14]. Two separate types of trajectories in joint space were evaluated i.e. lower and higher-order polynomials. The functions for a lower-order polynomial are parabolic and cubic. Septic and nonic were analyzed as higher-order polynomials [15].

In [16], a concept of reconfiguration was applied to CDPR by attaching idler pulleys to the moving platform to enhance manipulation capabilities and cable tension distribution. A similar approach was employed in [17] by installing cable-and-pulley differentials on the moving platform. It aims to anticipate the complicated pulley kinematics due to modeling inaccuracies. In [18], the pulleys can be positioned at a set of possible reconfigurations via optimization. A systematic approach to design an optimal reconfigurable CDPR was presented in [19]. Reconfigurable CDPR has been used for several applications, such as search-and-rescue operations [20], medical rehabilitation [21], airplane industries [22], [23], and building constructions [24], [25], [26].

In [27], the mobile bases were combined with CDPR due to their excellent mobility performance and payload capacity. Four mobile bases are linked to the moving platform by four cables, which enables the robot to perform 4-DOF motion [28]. In [29], [30], and [31], four mobile bases were employed, each consisting of two cables. The eight cables are connected to the moving platform, which is equipped with a gripper. The robot can be easily reconfigured and adapted to the environment thanks to mobile bases. The passive and active mobile bases can adjust the geometry of the CDPR according to the environment. A planar mobile CDPR was developed in [32] using two mobile bases, each composed of two cables.

The four-wheeled mobile robots like in [33] and [34] are commonly used to support the CDPR since their symmetrical architecture poses better load-carrying capacity and good motion stability [35], [36]. According to [37], the robot's motion stability is the robot's ability to return to the balance state when influenced by the external forces/moments such that the robot performs a smooth motion. The methods for stability analysis mainly consist of static analysis [38], [39] and dynamic analysis [40]. The most common static and dynamic stability criterion is the Zero-Moment-Point (ZMP), which is widely applied by the legged-locomotion and wheeled-locomotion robot communities. ZMP defines the point on the ground where the sum of the horizontal components of moments caused by the gravity and inertia forces is zero. The robot is stable if the ZMP is located inside the support boundaries. The horizontal distance between the ZMP and the support boundaries represents the tendency of the robot to tip over; hence, the ZMP concept is most suitable for motion on the horizontal plane or planar motion. The tipping-over rate is generally determined in the form of the moment equilibrium equations in static rate. It is possible to define the tipping-over stability for the dynamic characteristics [41]. The quadruped robot developed in [42] can adjust the next foot position based on the ZMP location to maintain stability when it bumps into unpredictable terrain. It proves that, in general, the robot's stability depends on the position of the next support that can supply the necessary moments to counter the tipping over.

Inspired by the above ideas, the CDPR in this paper is developed using three four-wheeled mobile bases equipped with a vertical crane. The cable exit points' next position can be altered so that the CDPR can maintain its stability despite the sudden spike in cable tension. The CDPR will stay stable if the ZMP is located within the ground-front wheel contact point and the ground-rear wheel contact point of the mobile base. To keep the ZMP always within the predefined boundaries, the next position of the cable exit points is modified in two ways: (I) driving the mobile base back and forth and (II) moving the crane up and down. The kinetostatic models associated with both techniques are formulated and included in the ZMP computation, which is the major contribution of the paper. An optimization is performed to determine a set of positions of the cable exit point; hence, they can provide the required moments to prevent the robot from tipping, and a prescribed trajectory can be smoothly executed within the robot workspace. An experimental setup to confirm the reconfiguration models is prepared and the results corroborate the developed hypotheses. To the best of the authors' knowledge, although a number of researches have been dedicated to reconfigurable CDPR, considering the ZMP in reconfigurable CDPR by using the mobile base and crane to maintain stability has not been discussed yet. The main ideas developed in this paper are the use of mobile bases can help to enlarge the workspace and the proposed reconfiguration schemes can regulate the cable tensions to maintain the robot's stability.

This paper is organized as follows: Section II describes the robot architecture and its reconfiguration scenarios. Section III derives the kinetostatic model of the system. Section IV discusses the ZMP to evaluate the mobile base's and crane's stability when the end-effector follows a trajectory. Section V deals with the reconfiguration planning of the robot, the optimal position of the mobile bases and crane lengths being obtained along a pre-defined trajectory of the end-effector. Section VI presents the prototype development and experiment, and the results are presented and discussed in Section VII. Finally, the conclusions are summarized in Section VIII.

II. ROBOT DESCRIPTION AND RECONFIGURATION SCHEMES

The schematic and parameterization of a CDPR with three mobile cranes are shown in Fig. 1. The robot consists of

three mobile cranes of local coordinate $\mathcal{L}(O_i, u_i, v_i, w_i)$, where $i = 1, 2, 3$. Each mobile crane is located at the local origin O_i with distance ρ_i from the global origin O of global coordinate $\mathcal{F}(O, X, Y, Z)$, and the angle γ_i is measured counterclockwise from X-axis as depicted in Fig. 1(b).

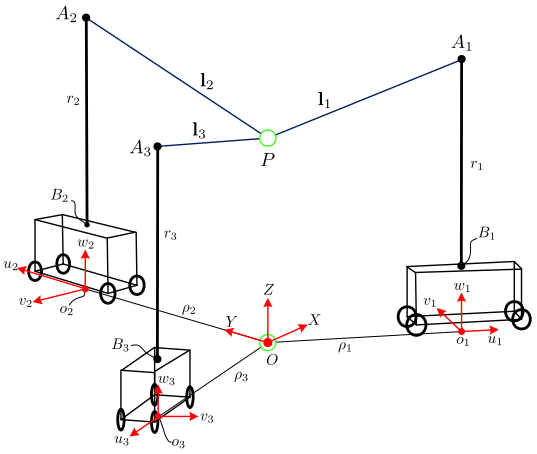

(a) Isometric view

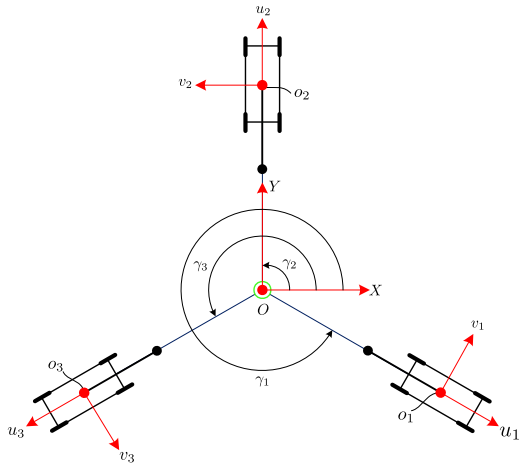

(b) Top view

FIGURE 1. Robot description.

The detailed vector diagram of each cable and the mobile base is illustrated in Fig. 2. The cables are linked from exit point A_i to point mass P. Exit point A_i is located at the pulley's center and connected to the crane at point A'_i. Point B_i is the connecting point from the mobile base to the crane.

Position vectors of exit point A_i in fixed coordinate ($\mathcal{F}$) are expressed by $\mathbf{a}_i^{\mathcal{F}}$, and it consists of the mobile base position $\rho_i^{\mathcal{F}}$ and crane length vectors $\mathbf{r}_i^{\mathcal{F}}$. Overall, vector $\mathbf{a}_i^{\mathcal{F}} = \left[a_{xi}, a_{yi}, a_{zi}\right]^T$ can be defined as follows:

$$\begin{aligned}\mathbf{a}_i^{\mathcal{F}} &= \rho_i^{\mathcal{F}} + \mathbf{r}_i^{\mathcal{F}} \\ &= \mathbf{v}_i^{\mathcal{F}} \rho_i + \mathbf{w}_i^{\mathcal{F}} r_i \end{aligned} \tag{1}$$

where ρ_i and r_i are, respectively, the mobile base position and the crane length. The unit vectors $\mathbf{v}_i^{\mathcal{F}}$ and $\mathbf{w}_i^{\mathcal{F}}$ express the direction of the mobile base and the crane, such that:

$$\mathbf{v}_i^{\mathcal{F}} = \begin{bmatrix} \cos\gamma_i \\ \sin\gamma_i \\ 0 \end{bmatrix} \qquad \mathbf{w}_i^{\mathcal{F}} = \begin{bmatrix} 0 \\ 0 \\ 1 \end{bmatrix} \tag{2}$$

where the orientation of all three mobile bases are respectively defined by: $\gamma_1 = 90°$, $\gamma_2 = 210°$, and $\gamma_3 = 330°$.

The end-effector is considered to be a point mass P, of coordinate vector $\mathbf{p} = [p_x, p_y, p_z]^T$. Therefore, the loop-closure equation corresponding to each cable can be defined as follows:

$$\mathbf{l}_i^{\mathcal{F}} = \rho_i^{\mathcal{F}} + \mathbf{r}_i^{\mathcal{F}} - \mathbf{p} \tag{3}$$

The cable length l_i is expressed as a function of the end-effector position, location of the mobile bases, and crane length as follows:

$$l_i = \left\| \mathbf{l}_i^{\mathcal{F}} \right\| = \sqrt{(\rho_i^{\mathcal{F}} + \mathbf{r}_i^{\mathcal{F}} - \mathbf{p})^T (\rho_i^{\mathcal{F}} + \mathbf{r}_i^{\mathcal{F}} - \mathbf{p})} \tag{4}$$

Accordingly, the unit vector of each cable $\mathbf{u}_i^{\mathcal{F}}$ is computed as follows:

$$\mathbf{u}_i^{\mathcal{F}} = \frac{\mathbf{l}_i^{\mathcal{F}}}{\left\| \mathbf{l}_i^{\mathcal{F}} \right\|} \tag{5}$$

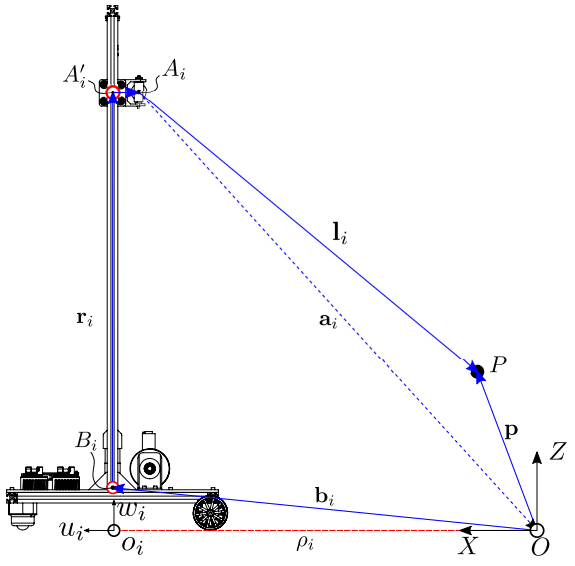

FIGURE 2. Geometric description of a mobile base.

In this paper, the concept of reconfiguration is introduced to be applicable to the developed CDPR; hence, its workspace can be enlarged and tipping can be avoided when tracking a given trajectory. Two reconfiguration scenarios are defined by moving the crane up and down and by driving the mobile base forward and backward, as follows:

1) **Reconfiguration I: mobile base reconfiguration**
The three mobile bases are driven forward and backward such that their position reaches a minimum and maximum distances, i.e. $\rho_{i_{min}} = 1m$ and $\rho_{i_{max}} = 1.5m$, as shown in Fig. 3(a) by blue arrows).

2) **Reconfiguration II: crane reconfiguration**
The crane is retracted and extended up to its minimum and maximum lengths, respectively, i.e. $r_{i_{min}} = 0.53m$ and $r_{i_{max}} = 0.83m$, as shown in Fig. 3(b) by blue arrows.

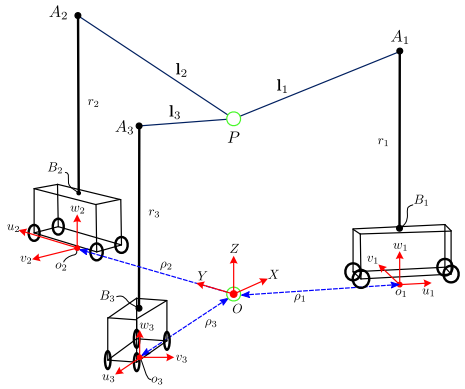

(a) Reconfiguration I (mobile base)

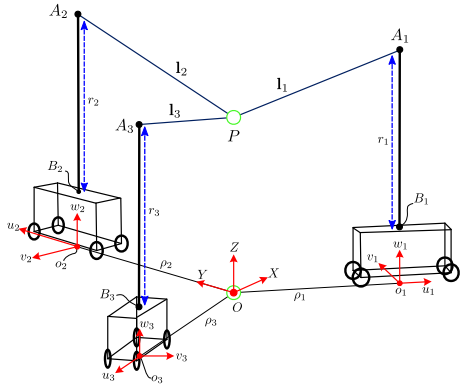

(b) Reconfiguration II (crane)

FIGURE 3. Reconfiguration schemes.

III. KINETOSTATIC MODEL

A. KINETOSTATIC MODEL OF END-EFFECTOR

Here, the robot is supposed to move at relatively low velocities and accelerations and be stable within a large workspace. The cables are assumed to be non-elastic and mass-less. As a consequence, the dynamic effects on the system are omitted. The equation of static equilibrium at point P is expressed as follows:

$$\mathbf{W}\tau + \mathbf{w}_e = \mathbf{0} \tag{6}$$

where $\tau = [\tau_1, \tau_2, \tau_3]^T$ is the cable tensions vector, and $\mathbf{w}_e = [0, 0, -mg]^T$ is the gravitational force acting at point mass P. The gravity vector is denoted by $\mathbf{g} = [0, 0, -g]^T$ where $g = 9.8\,m.s^{-1}$. Since the wrench matrix $\mathbf{W}$ is a 3×3 square matrix, then the cable tensions can be computed as follows:

$$\tau = -\mathbf{W}^{-1}\mathbf{w}_e \tag{7}$$

and the cable force $\mathbf{f}_i$ can be expressed as follows:

$$\mathbf{f}_i = \mathbf{u}_i^{\mathcal{F}}\tau_i \tag{8}$$

The wrench matrix $\mathbf{W}$ of reconfiguration scenarios I and II are computed from the transpose of the Jacobian matrices, respectively, as:

$$\mathbf{W} = \begin{cases} \mathbf{J}_{\mathrm{I}}^T, & \text{for reconfiguration scheme I,} \\ \mathbf{J}_{\mathrm{II}}^T, & \text{for reconfiguration scheme II.} \end{cases} \tag{9}$$

In the concept of reconfiguration applied to the developed robot, the mobile bases, and the cranes are allowed to move when the cables are in operation. Hence, the mobile bases and the cranes will travel with velocities $\dot{\rho} = [\dot{\rho_1}, \dot{\rho_2}, \dot{\rho_3}]^T$ and $\dot{\mathbf{r}} = [\dot{r_1}, \dot{r_2}, \dot{r_3}]^T$, respectively. If the cable velocity vector is $\dot{\mathbf{l}} = \left[\dot{l_1}, \dot{l_2}, \dot{l_3}\right]^T$, Eq. (3) can be derived with respect to time to obtain the following relationship:

$$\mathbf{A}\dot{\mathbf{l}} = \mathbf{B}\dot{\rho} + \mathbf{C}\dot{\mathbf{r}} - \dot{\mathbf{p}} \tag{10}$$

where matrices $\mathbf{A}$, $\mathbf{B}$, and $\mathbf{C}$ are respectively defined as follows:

$$\mathbf{A} = \begin{bmatrix} \mathbf{u}_1^{\mathcal{F}} & \mathbf{u}_2^{\mathcal{F}} & \mathbf{u}_3^{\mathcal{F}} \end{bmatrix} \tag{11a}$$
$$\mathbf{B} = \begin{bmatrix} \mathbf{v}_1^{\mathcal{F}} & \mathbf{v}_2^{\mathcal{F}} & \mathbf{v}_3^{\mathcal{F}} \end{bmatrix} \tag{11b}$$
$$\mathbf{C} = \begin{bmatrix} \mathbf{w}_1^{\mathcal{F}} & \mathbf{w}_2^{\mathcal{F}} & \mathbf{w}_3^{\mathcal{F}} \end{bmatrix} \tag{11c}$$

Equation (10) should be treated separately for each reconfiguration scenario to determine the Jacobian matrices $\mathbf{J}_{\mathrm{I}}$ and $\mathbf{J}_{\mathrm{II}}$, as follows:

1) **Kinetostatic of reconfiguration I**
In this reconfiguration scenario, the three mobile bases can adjust their position while the cranes are maintained to be constant, therefore Eq. (10) becomes:

$$\mathbf{A}\dot{\mathbf{l}} = \mathbf{B}\dot{\rho} - \dot{\mathbf{p}} \tag{12}$$

To discard the velocity term $\mathbf{B}\dot{\rho}$ in Eq. (12), a diagonal and invertible matrix $\mathbf{E}$ is introduced. Matrix $\mathbf{E}$ is composed of the mobile base velocities as follows:

$$\mathbf{E} = \begin{bmatrix} \dfrac{\dot{\rho_3}}{\dot{\rho_1}} & 0 & 0 \\ 0 & \dfrac{\dot{\rho_3}}{\dot{\rho_2}} & 0 \\ 0 & 0 & 1 \end{bmatrix} \tag{13}$$

By multiplying Eq. (12) with diagonal matrix $\mathbf{E}$, the velocity vector of the mobile base $\dot{\rho}$ is eliminated and the cable velocity can be computed, such that:

$$\begin{aligned} \mathbf{A}\mathbf{E}\dot{\mathbf{l}} &= -\mathbf{E}\,\dot{\mathbf{p}} \\ \dot{\mathbf{l}} &= -\mathbf{E}^{-1}\mathbf{A}^{-1}\mathbf{E}\,\dot{\mathbf{p}} \\ \dot{\mathbf{l}} &= -\mathbf{J}_{\mathrm{I}}\,\dot{\mathbf{p}} \end{aligned} \tag{14}$$

where $\mathbf{J}_{\mathrm{I}}$ is the Jacobian matrix of reconfiguration scenario I that maps the end-effector velocity into the cable velocities by considering the mobile base velocities.

2) **Kinetostatic of reconfiguration II**

The crane lengths can be moved up and down and simultaneously keep the mobile base position constant. As a consequence, Eq. (10) can be written as follows:

$$\mathbf{A}\dot{\mathbf{l}} = \mathbf{C}\dot{\mathbf{r}} - \dot{\mathbf{p}} \tag{15}$$

A matrix $\mathbf{F}$ is introduced to remove the velocity term $\mathbf{C}\dot{\mathbf{r}}$ in Eq. (15). Matrix $\mathbf{F}$ is a diagonal and invertible matrix that consists of the crane velocities as follows:

$$\mathbf{F} = \begin{bmatrix} \dot{r}_2\dot{r}_3 & 0 & 0 \\ 0 & \dot{r}_1\dot{r}_3 & 0 \\ 0 & 0 & -2\dot{r}_1\dot{r}_2 \end{bmatrix} \tag{16}$$

and Eq. (15) can be expressed as:

$$\begin{aligned} \mathbf{A}\mathbf{F}\dot{\mathbf{l}} &= -\mathbf{F}\,\dot{\mathbf{p}} \\ \dot{\mathbf{l}} &= -\mathbf{F}^{-1}\mathbf{A}^{-1}\mathbf{F}\,\dot{\mathbf{p}} \\ \dot{\mathbf{l}} &= -\mathbf{J}_{\mathrm{II}}\,\dot{\mathbf{p}} \end{aligned} \tag{17}$$

Matrix $\mathbf{J}_{\mathrm{II}}$ maps the end-effector velocity into the cable velocities by taking into account the crane velocities.

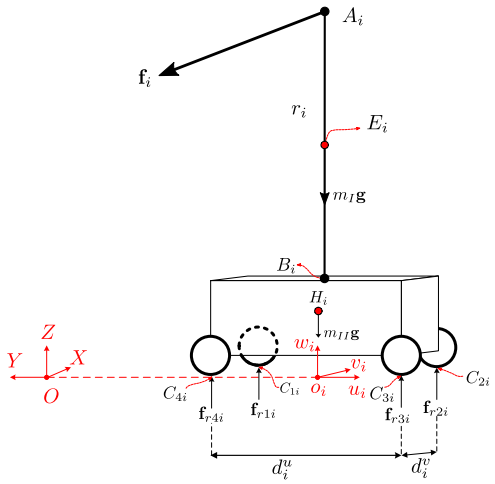

(a) Isometric view

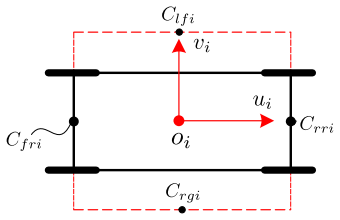

(b) Top view

FIGURE 4. Free body diagram of mobile base.

B. STATIC MODEL OF MOBILE BASE

Three mobile cranes should satisfy the static equilibrium condition during the end-effector movement. The free-body diagram of the i-th mobile crane is illustrated in Fig. 4. The mobile crane is said to be tipping if it turns over about the axis v_i. The frontal and rear reaction forces between the ground and the wheels can be respectively written, as follows:

$$\begin{aligned} \mathbf{f}_{fri} &= \mathbf{f}_{r1i} + \mathbf{f}_{r4i} \\ \mathbf{f}_{rri} &= \mathbf{f}_{r2i} + \mathbf{f}_{r3i} \end{aligned} \tag{18}$$

where $\mathbf{f}_{rji}$ is the reaction force of the k-th wheel as shown in Fig. 4(a). Based on Newton's law of motion, the force and moment equilibrium at point O are defined as follows:

$$\sum \mathbf{f} = 0 \quad \mathbf{f}_{fri} + \mathbf{f}_{rri} + m_I\,\mathbf{g} + m_{II}\,\mathbf{g} + \mathbf{f}_i = 0 \tag{19}$$

$$\begin{aligned} \sum \mathbf{M}_O = 0 \quad & \mathbf{c}_{fri} \times \mathbf{f}_{fri} + \mathbf{c}_{rri} \times \mathbf{f}_{rri} + \mathbf{a}_i^{\mathcal{F}} \times \mathbf{f}_i \\ & + m_I.\mathbf{e}_i^{\mathcal{F}} \times \mathbf{g} + m_{II}.\mathbf{h}_i^{\mathcal{F}} \times \mathbf{g} = 0 \end{aligned} \tag{20}$$

where m_I and m_{II} are masses of the crane and mobile base, respectively. Their gravitational forces act at points E and H. $\mathbf{h}_i^{\mathcal{F}}$ and $\mathbf{e}_i^{\mathcal{F}}$ are the position vectors of the center of gravity H for the mobile base and E for the crane. $\mathbf{c}_{fri}$ and $\mathbf{c}_{rri}$ are the position vectors from the origin O to the frontal and rear sides of the mobile crane. $\mathbf{c}_{fri}$ and $\mathbf{c}_{rri}$ are defined as follows:

$$\begin{aligned} \mathbf{c}_{fri} &= \begin{bmatrix} \cos(\gamma_i)(\rho_i - L/2) \\ \sin(\gamma_i)(\rho_i - L/2) \\ 0 \end{bmatrix} \\ \mathbf{c}_{rri} &= \begin{bmatrix} \cos(\gamma_i)(\rho_i + L/2) \\ \sin(\gamma_i)(\rho_i + L/2) \\ 0 \end{bmatrix} \end{aligned} \tag{21}$$

The vertical components of frontal and rear reaction forces become:

$$f_{rri}^z = m_I g + m_{II} g - f_i^z - f_{fri}^z \tag{22}$$

$$\begin{aligned} f_{fri}^z = {} & \left((e_i^y - c_{rri}^y)m_I g + (h_i^y - c_{rri}^y)m_{II} g \right. \\ & \left. + (c_{rri}^y - a_i^y)f_i^z + a_i^z f_i^y\right)/\left(c_{fri}^y - c_{rri}^y\right) \end{aligned} \tag{23}$$

Equations (22) and (23) illustrate the effect of external forces acting on the cables on the stability of mobile cranes, which is defined by the value of reaction forces. It turns out that as the end-effector moves about a given path, the external forces may pull the cables, which eventually cause the mobile cranes to undergo tipping.

IV. STABILITY BASED ON ZMP

When the mobile bases move and execute a given task, the reaction forces are exerted between the wheels and the ground at the contact point. These reaction forces will be null if the robot tips over. Therefore, the tipping moment acting on the contact point is considered the moment's component [43].

In this paper, Zero Moment Point (ZMP) is used to evaluate the robot's stability, which can be defined as a point within the mobile bases where the sum of moments due to frontal and rear reaction forces is null. ZMP is expressed in the local coordinate $\mathcal{L}(u_i, v_i, w_i)$. Then, the cable force expressed in the local coordinate is as follows:

$$\mathbf{f}_i^{\mathcal{L}} = \begin{bmatrix} f_i^u \\ f_i^v \\ f_i^w \end{bmatrix} = \begin{bmatrix} f_i^x \cos(\gamma_i) + f_i^y \sin(\gamma_i) \\ -f_i^x \sin(\gamma_i) + f_i^y \cos(\gamma_i) \\ f_i^z \end{bmatrix} \tag{24}$$

At this instant, ZMP is applied to ensure the mobile crane is in static equilibrium while the end-effector moves along a prescribed path. As a result, the sum of moments at point o_i can be formulated for tipping analysis as follows:

$$\mathbf{M}_{o_i} - (f_{fri} + f_{rri}) \times d_i = 0 \tag{25}$$

where $\mathbf{d}_i$ is the vector position from the origin o_i to the edge of the mobile crane. The mobile crane will tip over about axis v_i, which means that ZMP should be maintained between the points C_{1i} and C_{2i} or within the distance d_i^u as shown in FIGURE 4(b). From Equation (25), d_i^u is defined as follows:

$$d_i^u = \frac{a_i^u f_i^w - a_i^w f_i^u - m_I e_i^u g}{f_{fri}^w + f_{rri}^w} \tag{26}$$

Static-Feasible-Workspace [44] is characterized as the set of end-effector poses for which the cables can maintain the static equilibrium under external force. The wrench is maintained to be positive in Static-Feasible-Workspace since the cable can be counteracted by the force applied onto the end-effector. In this section, the Static-Feasible-Workspace of the robot is computed when the robot is in non-reconfiguration state by solving Eq. (7), as shown in Fig. 5(a). To ensure that the end-effector can perform a task while the mobile cranes are in static equilibrium, point P must work inside the Static-Feasible-Workspace. The Static-Tipping-Free-Workspace can be generated by including the ZMP condition in the robot operation, i.e. by taking into account Eq. (23) into Eq. (7), as shown in Fig. 5(b). The size of the Static-Tipping-Free-Workspace is smaller, limiting the robot's movement. To deal with this issue, the reconfiguration schemes are introduced in Section II, which can simultaneously enlarge the working coverage and manage the robot's stability.

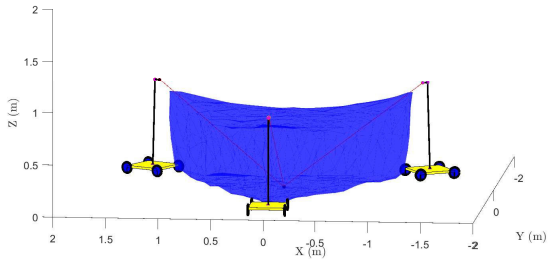

(a) Static Feasible Workspace

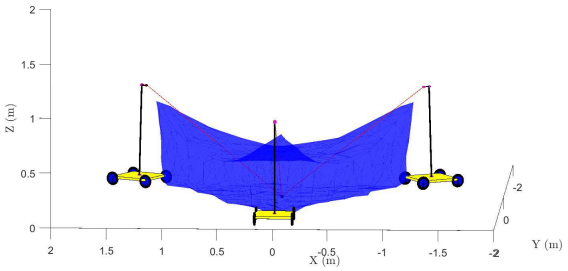

(b) Static Tipping-Free Workspace

FIGURE 5. Workspaces.

The Static Feasible Workspace in Fig. 5(a): Point mass $m = 1kg$, crane's mass $m_I = 1.853kg$ and mobile base's mass $m_{II} = 3.093kg$. The tension limit is $1N \leq \tau_i \leq 25N$.

V. RECONFIGURATION OPTIMIZATION

A trajectory, as shown in Fig. 6, is generated to assess the performance of the developed prototype, which will be demonstrated in Section VI. The prescribed trajectory is a succession of three segments from the first segment at $P_0 - P_1$ for $t = 0 - 5s$, the second segment at $P_1 - P_2$ for $t = 5 - 15s$, and the third segment at $P_2 - P_3$ for $t = 15 - 25s$. A fifth-order polynomial is used to obtain smooth velocity and acceleration profiles for each segment of the trajectory. Both reconfiguration schemes I and II will execute this trajectory. The trajectory is discretized into 300 equidistant points P. At each point, a set of positions of three mobile bases and a set of the length of three cranes (denoted by ρ_i and r_i, respectively) should be determined via optimization. The vectors consisting of the decision variables of reconfiguration schemes I and II are written as follows:

$$\mathbf{x} = \begin{cases} [\,\rho_1, \rho_2, \rho_3\,], & \text{for reconfiguration scheme I,} \\ [\,r_1, r_2, r_3\,], & \text{for reconfiguration scheme II.} \end{cases} \tag{27}$$

The boundaries of decision variables are based on the developed prototype, given as follows:

$$\begin{aligned} 1m \leq \rho_1, \rho_2, \rho_3 \leq 1.5m \\ 0.53m \leq r_1, r_2, r_3 \leq 0.83m \end{aligned} \tag{28}$$

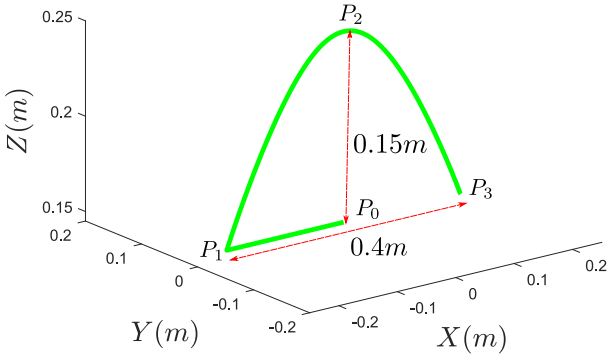

FIGURE 6. Testing trajectory.

Cable tensions have a big influence on the robot's static equilibrium. Likewise, cable velocities have a significant impact on the robot's motion. The optimization problem aims to simultaneously minimize cable tensions and velocities to improve the robot's stability and motion smoothness. The motor mounted to the winch coils the cable with maximum cable velocity up to 0.015 m/s. Based on this technical requirement, the cable velocity becomes more important to reduce the motor burden, therefore, the weighting factor

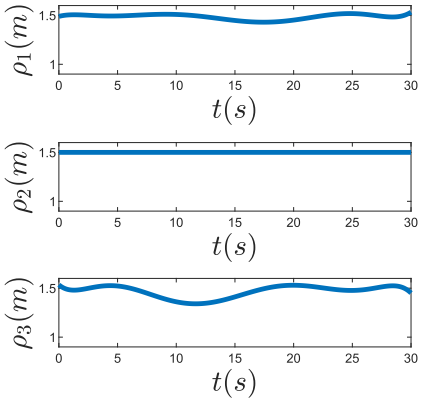

(a) Reconfiguration I

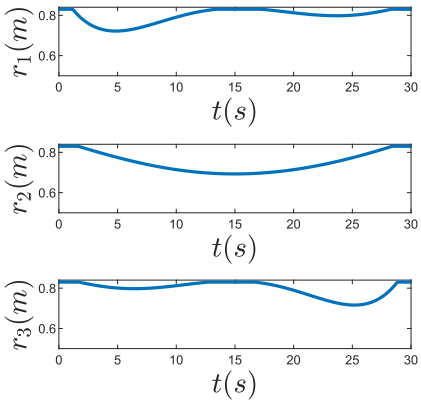

(b) Reconfiguration II

FIGURE 7. Optimization results.

$\lambda = 0.75$ is introduced in the formulation of the objective function as follows:

$$\mathcal{U}(\mathbf{x}) = (1-\lambda)\|\tau(\mathbf{x})\| + \lambda\|\dot{l}(\mathbf{x})\| \tag{29}$$

The use of a mobile base as a frame of CDPR, exposes a great risk of instability, which leads the robot to tumble. The robot stability becomes an important element during the optimization process at each point P of the trajectory. To satisfy this condition, the ZMP should always stay within the allowable distance d_i^u, representing the distance between the ground-front wheel contact point c_{fri}^u and the ground-rear wheel contact point c_{rri}^u. Eventually, the design problem can be formulated as follows:

$$\begin{aligned} \text{Find}: &\ \mathbf{x} \\ \text{Minimize}: &\ \mathcal{U}(\mathbf{x}) \\ \text{Subject to}: &\ c_{fri}^u \le d_i^u \le c_{rri}^u \end{aligned} \tag{30}$$

The optimum results along the prescribed trajectory are presented in Fig. 7. During reconfiguration scheme I, the mobile bases will change their positions following the optimal results shown in Fig. 7(a). Only the first and third mobile bases move. During reconfiguration scheme II, the cranes move up and down based on the optimal data given in Fig. 7(b). These designs will accordingly change the cable exit points that can prevent the robot from tipping and generate lower cable tensions. The experimentation of these designs is presented in Section VI

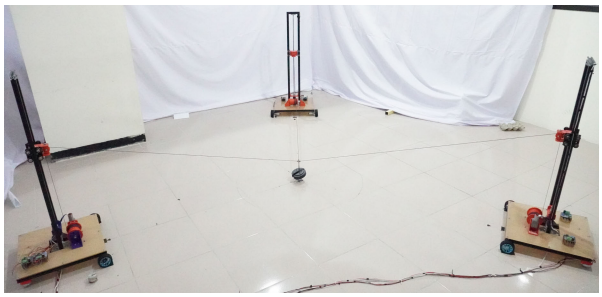

(a) Isometric view

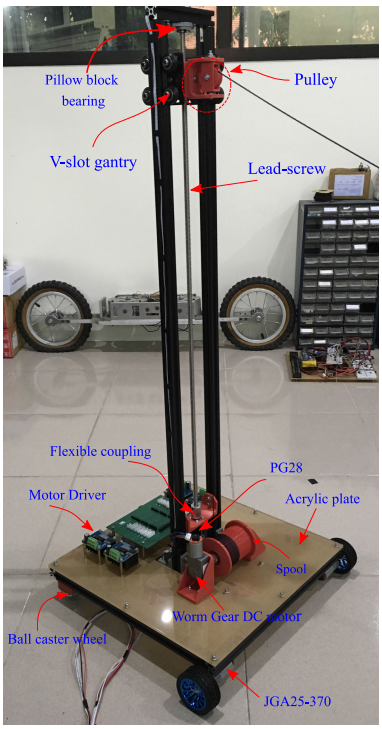

(b) Transmission

FIGURE 8. Developed prototype.

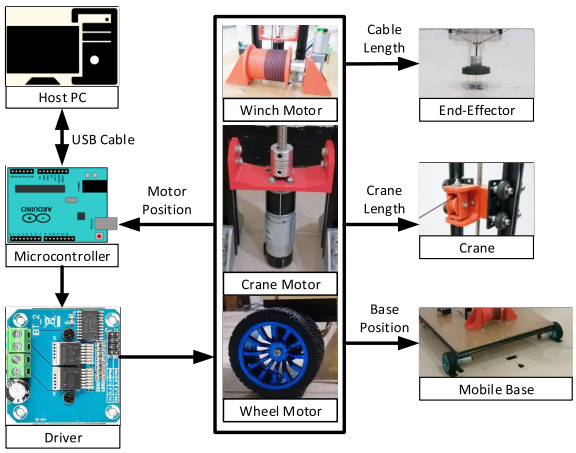

FIGURE 9. Control architecture.

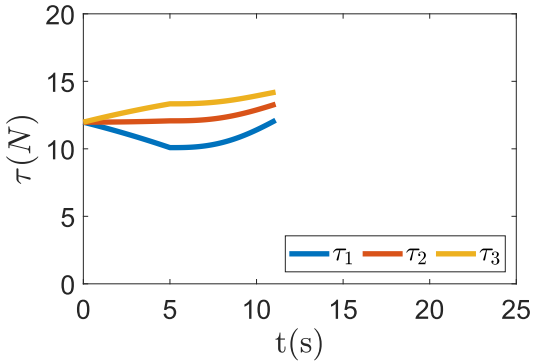

FIGURE 10. Computational results of tension distribution without reconfiguration (tipping).

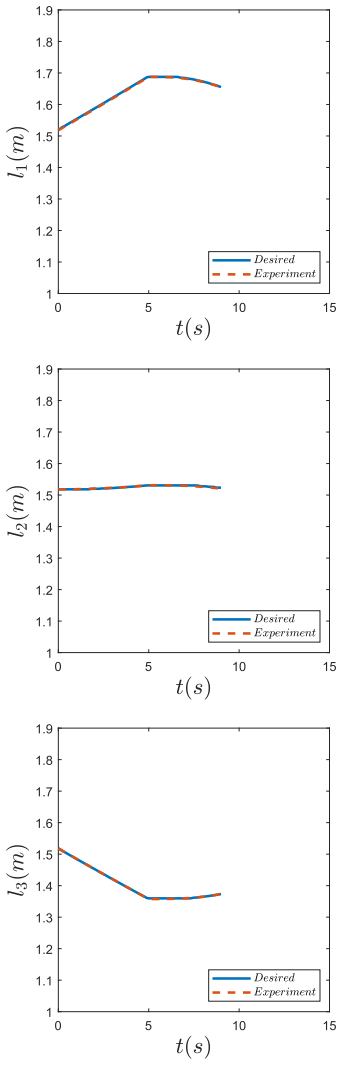

FIGURE 11. Experimental results without reconfiguration.

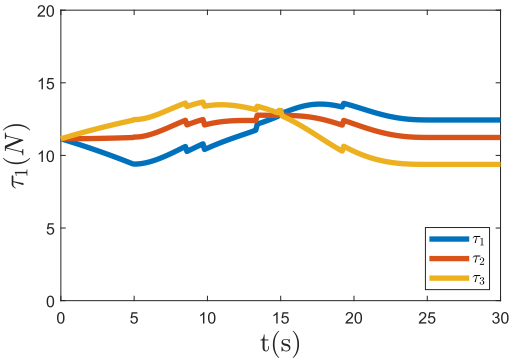

(a) Reconfiguration I

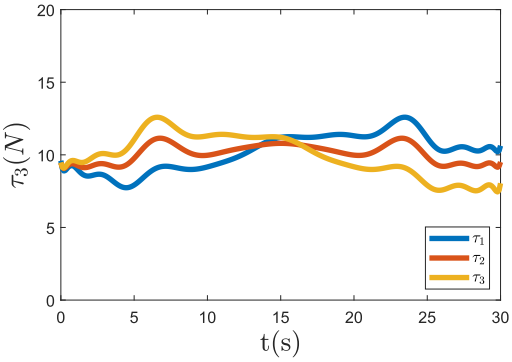

(b) Reconfiguration II

FIGURE 12. Computational results of tension distribution with reconfiguration.

VI. PROTOTYPE AND EXPERIMENT

The prototype of a cable-driven parallel robot with multiple mobile bases has been manufactured as shown in Fig. 8(a), and the transmission system of a mobile base is presented in Fig. 8(b). Each mobile base carries four actuators; namely: two actuators are used to drive the frontal wheels to move the mobile base, one actuator is used to actuate the lead screw to provide the crane motion at which the pulley is attached, and another one is to rotate the custom-made winch to coil the cables. The control system of the prototype is presented in Fig. 9, which is composed of a PC (equipped with ©MATLAB), a microcontroller, a motor driver, a transmission assembly divided into a winch motor with gearbox, a crane motor with lead screw, and the wheel motors.

VII. RESULTS AND DISCUSSION

Initially, the robot was tested to move along the generated trajectory without adjusting the crane and mobile base. The computation of the tension distribution is shown in Fig. 10. The third cable tension jumps to $\tau_3 = 16.5\ N$, making the mobile base unstable and terminating the task around $t = 9\ s$. The third mobile base cannot handle high cable tension and finally collapses since the ZMP is not within the support boundaries. This robot's instability is corroborated by the experiment demonstrated in this video.[1] Figures 11(a)-(c) depict the experimental results between the

[1] Experiment of Non-reconfiguration

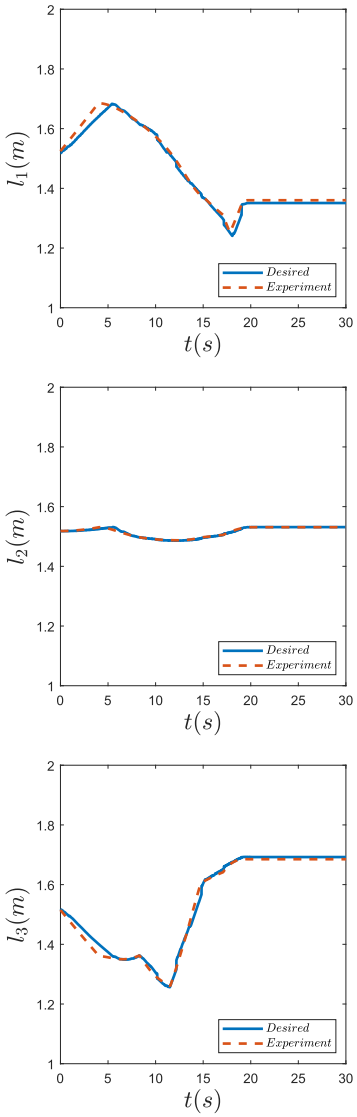

FIGURE 13. Results from the experiments of reconfiguration I.

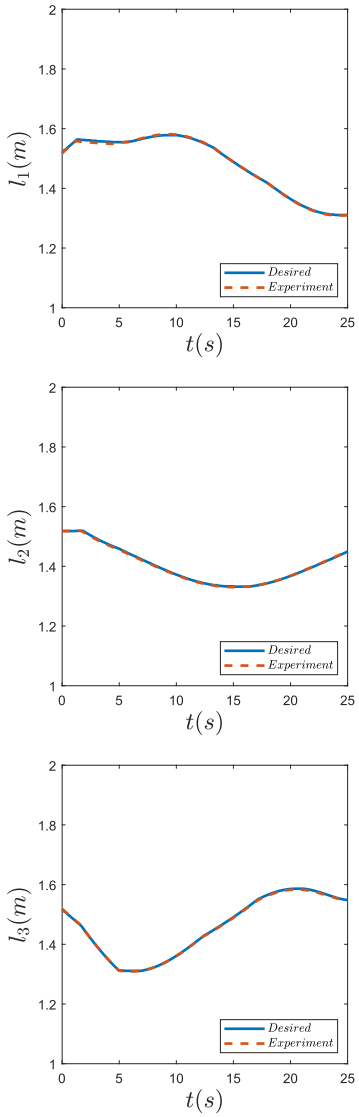

FIGURE 14. Results from the experiments of reconfiguration II.

desired and measured cable lengths when the robot moves without changing its cable exit points.

Then, two reconfiguration schemes were tested empirically as the end-effector executed the same trajectory. The tensions of the three cables are computed for reconfiguration schemes I and II, and their distributions are respectively presented in Figs. 12(a) and 12(b). Optimizing the mobile base position and the crane length reduces the cable tensions compared to the cable tensions obtained with the non-reconfiguration system. None of the mobile base turnover since the ZMP always stays within the support boundaries denoted by d_i^u, which justifies that the robot is able to maintain its stability during the task. The demonstration videos are provided to show the reconfiguration I and II.[2] Figures 13 and 14 depict the differences between the desired and measured cable lengths of reconfigurations I and II,

[2]Experiment of Reconfiguration

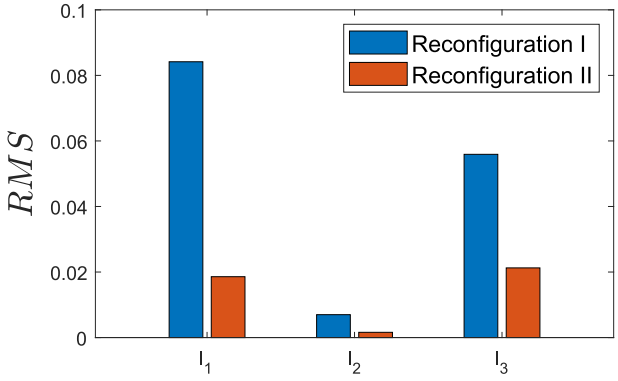

FIGURE 15. RMS of the cable length error.

respectively. The root mean square errors between the desired and obtained cable lengths during the reconfigurations I and II experiments are presented in Fig. 15. Despite the fact that

errors exist, it shows that the completed experiments confirm the kinetostatic models derived for both reconfiguration schemes in Eqs. (14) and (17). The errors of cable lengths in reconfiguration I are higher than the ones in reconfiguration II, since driving the mobile bases that act as a frame for the whole robot will induce external moments to the end-effector that will eventually reduce the robot's rigidity. The slippage between the wheel and the ground might also contribute to it.

Cable tensions of reconfiguration II are lower than those of reconfiguration I. Likewise, the root mean square errors of cable length of reconfiguration II (less than 0.02) are significantly lower than those of reconfiguration I. According to these results, altering the crane will be more beneficial than changing the mobile base position, which means that reconfiguration II is more efficient for technical use.

VIII. CONCLUSION

In this paper, the stability of a CDPR using three mobile cranes was investigated based on the concept of ZMP. The robot will remain stable if ZMP always stays within the specified support boundaries. Thus, the next positions of the cable exit point were shifted by implementing two reconfiguration schemes for the robot: (I) driving the mobile base forward and backward and (II) moving the crane up and down. Kinetostatic models of both schemes were derived, and the robot's workspace was plotted by considering the ZMP. A trajectory traced by the end-effector was generated by using the fifth-degree polynomial. Following this trajectory, the next positions of cable exit points were always changed, represented by the continuous change of the mobile base position and the crane length of the reconfiguration schemes I and II, respectively. An optimization problem was formulated and solved to define the set of mobile base positions and the crane lengths such that the whole system remains in equilibrium. A prototype of the CDPR using three mobile cranes was fabricated. An experiment was performed on the developed prototype, and it confirmed that both reconfiguration schemes were able to prevent the robot from tipping over when executing a given task. The results also revealed that the cable tensions and the error in cable lengths for reconfiguration II are lower than those for reconfiguration I, which shows that reconfiguration II gives better results in terms of robot stability. The future research direction will consider reconfigurable mobile robots with adjustable width and length to improve the mechanical stability of mobile CDPR.

REFERENCES

[1] A. Pott, H. Mütherich, W. Kraus, V. Schmidt, P. Miermeister, and A. Verl, "IPAnema: A family of cable-driven parallel robots for industrial applications," in *Cable-Driven Parallel Robots*. Berlin, Germany: Springer, 2013, pp. 119–134.

[2] J. Lamaury, M. Gouttefarde, A. Chemori, and P.-É. Hervé, "Dual-space adaptive control of redundantly actuated cable-driven parallel robots," in *Proc. IEEE/RSJ Int. Conf. Intell. Robots Syst.*, Nov. 2013, pp. 4879–4886.

[3] P. Tempel, P.-E. Herve, O. Tempier, M. Gouttefarde, and A. Pott, "Estimating inertial parameters of suspended cable-driven parallel robots—Use case on CoGiRo," in *Proc. IEEE Int. Conf. Robot. Autom. (ICRA)*, May 2017, pp. 6093–6098.

[4] F. Okoli, Y. Lang, O. Kermorgant, and S. Caro, "Cable-driven parallel robot simulation using gazebo and ros," in *ROMANSY 22—Robot Design, Dynamics and Control*. Cham, Switzerland: Springer, 2019, pp. 288–295.

[5] S. Abdolshah, D. Zanotto, G. Rosati, and S. K. Agrawal, "Optimizing stiffness and dexterity of planar adaptive cable-driven parallel robots," *J. Mech. Robot.*, vol. 9, no. 3, Jun. 2017, Art. no. 031004.

[6] H. Lamine, L. Romdhane, H. Saafi, and S. Bennour, "Design-to-Workspace synthesis of a cable robot used in legs training machine," *Robotica*, vol. 38, no. 9, pp. 1703–1714, Sep. 2020.

[7] A. Pott, *Cable-Driven Parallel Robots*. Cham, Switzerland: Springer, 2018.

[8] M. Gouttefarde, J.-P. Merlet, and D. Daney, "Wrench-feasible workspace of parallel cable-driven mechanisms," in *Proc. IEEE Int. Conf. Robot. Autom.*, Apr. 2007, pp. 1492–1497.

[9] H. Hussein, J. C. Santos, J.-B. Izard, and M. Gouttefarde, "Smallest maximum cable tension determination for cable-driven parallel robots," *IEEE Trans. Robot.*, vol. 37, no. 4, pp. 1186–1205, Aug. 2021.

[10] T. Rasheed, P. Long, D. Marquez-Gamez, and S. Caro, "Available wrench set for planar mobile cable-driven parallel robots," in *Proc. IEEE Int. Conf. Robot. Autom. (ICRA)*, May 2018, pp. 962–967.

[11] T. Rasheed, P. Long, and S. Caro, "Wrench-feasible workspace of mobile cable-driven parallel robots," *J. Mech. Robot.*, vol. 12, no. 3, 2020, Art. no. 031009.

[12] R. Verhoeven, "Analysis of the workspace of tendon-based Stewart platforms," Inst. Mechtron. Syst. Dyn., Univ. Duisburg-Essen, Duisburg, Germany, 2004.

[13] C. Gosselin, "Global planning of dynamically feasible trajectories for three-DOF spatial cable-suspended parallel robots," in *Cable-Driven Parallel Robots*. Berlin, Germany: Springer, 2013, pp. 3–22.

[14] Y. Fang, J. Hu, W. Liu, Q. Shao, J. Qi, and Y. Peng, "Smooth and time-optimal S-curve trajectory planning for automated robots and machines," *Mechanism Mach. Theory*, vol. 137, pp. 127–153, Jul. 2019.

[15] P. A. Parikh, R. Trivedi, and J. Dave, "Trajectory planning for the five degree of freedom feeding robot using septic and nonic functions," *Int. J. Mech. Eng. Robot. Res.*, vol. 9, no. 7, pp. 1043–1050, 2020.

[16] T. D. Nguyen, P. T. Phan, and T. T. Nguyen, "Design dynamic models for cable robot spraying pesticides in agricultural production," *Int. J. Mech. Eng. Robot. Res.*, vol. 9, no. 4, pp. 516–520, 2020.

[17] R. Wang and Y. Li, "Analysis and multi-objective optimal design of a planar differentially driven cable parallel robot," *Robotica*, vol. 39, no. 12, pp. 2193–2209, Dec. 2021.

[18] L. Gagliardini, S. Caro, M. Gouttefarde, and A. Girin, "Discrete reconfiguration planning for cable-driven parallel robots," *Mechanism Mach. Theory*, vol. 100, pp. 313–337, Jan. 2016.

[19] G. Rosati, D. Zanotto, and S. K. Agrawal, "On the design of adaptive cable-driven systems," *J. Mech. Robot.*, vol. 3, no. 2, 2011, Art. no. 021004.

[20] S. Tadokoro, R. Verhoeven, M. Hiller, and T. Takamori, "A portable parallel manipulator for search and rescue at large-scale urban earthquakes and an identification algorithm for the installation in unstructured environments," in *Proc. IEEE/RSJ Int. Conf. Intell. Robots Syst., Hum. Environ. Friendly Robots High Intell. Emotional Quotients*, Feb. 1999, pp. 1222–1227.

[21] D. Zanotto, G. Rosati, S. Minto, and A. Rossi, "Sophia-3: A semiadaptive cable-driven rehabilitation device with a tilting working plane," *IEEE Trans. Robot.*, vol. 30, no. 4, pp. 974–979, Aug. 2014.

[22] D. Q. Nguyen and M. Gouttefarde, "Study of reconfigurable suspended cable-driven parallel robots for airplane maintenance," in *Proc. IEEE/RSJ Int. Conf. Intell. Robots Syst.*, Sep. 2014, pp. 1682–1689.

[23] P. Bosscher, R. L. Williams, L. S. Bryson, and D. Castro-Lacouture, "Cable-suspended robotic contour crafting system," *Autom. Construct.*, vol. 17, no. 1, pp. 45–55, Nov. 2007.

[24] I. Vukorep, "Autonomous big-scale additive manufacturing using cable-driven robots," in *Proc. Int. Symp. Autom. Robot. Construct. (IAARC)*, vol. 34, 2017, pp. 254–259.

[25] T. Bruckmann, C. Reichert, M. Meik, P. Lemmen, A. Spengler, H. Mattern, and M. König, "Concept studies of automated construction using cable-driven parallel robots," in *Cable-Driven Parallel Robots*. Cham, Switzerland: Springer, 2018, pp. 364–375.
[26] R. Boumann, P. Lemmen, R. Heidel, and T. Bruckmann, "Optimization of trajectories for cable robots on automated construction sites," in *Proc. 37th Int. Symp. Autom. Robot. Construct. (ISARC)*, Oct. 2020, pp. 465–472.
[27] T. Rasheed, P. Long, A. S. Roos, and S. Caro, "Optimization based trajectory planning of mobile cable-driven parallel robots," in *Proc. IEEE/RSJ Int. Conf. Intell. Robots Syst. (IROS)*, Nov. 2019, pp. 6788–6793.
[28] B. Zi, J. Lin, and S. Qian, "Localization, obstacle avoidance planning and control of a cooperative cable parallel robot for multiple mobile cranes," *Robot. Comput.-Integr. Manuf.*, vol. 34, pp. 105–123, Aug. 2015.
[29] N. Pedemonte, T. Rasheed, D. Marquez-Gamez, P. Long, É. Hocquard, F. Babin, C. Fouché, G. Caverot, A. Girin, and S. Caro, "FASTKIT: A mobile cable-driven parallel robot for logistics," in *Advances in Robot Kinematics*. Cham, Switzerland: Springer, 2020, pp. 141–163.
[30] T. Rasheed, P. Long, D. Marquez-Gamez, and S. Caro, "Kinematic modeling and twist feasibility of mobile cable-driven parallel robots," in *Advances in Robot Kinematics*. Cham, Switzerland: Springer, 2019, pp. 410–418.
[31] C. Alias, I. Nikolaev, E. G. Correa Magallanes, and B. Noche, "An overview of warehousing applications based on cable robot technology in logistics," in *Proc. IEEE Int. Conf. Service Oper. Logistics, Informat. (SOLI)*, Jul. 2018, pp. 232–239.
[32] T. Rasheed, P. Long, D. Marquez-Gamez, and S. Caro, "Tension distribution algorithm for planar mobile cable-driven parallel robots," in *Cable-Driven Parallel Robots*. Cham, Switzerland: Springer, 2018, pp. 268–279.
[33] E. Karamipour, S. F. Dehkordi, and M. H. Korayem, "Reconfigurable mobile robot with adjustable width and length: Conceptual design, motion equations and simulation," *J. Intell. Robot. Syst.*, vol. 99, nos. 3–4, pp. 797–814, Sep. 2020.
[34] M. H. Korayem and S. F. Dehkordi, "Motion equations of cooperative multi flexible mobile manipulator via recursive Gibbs–Appell formulation," *Appl. Math. Model.*, vol. 65, pp. 443–463, Jan. 2019.
[35] H. Tan, L. Nurahmi, B. Pramujati, and S. Caro, "On the reconfiguration of cable-driven parallel robots with multiple mobile cranes," in *Proc. 5th Int. Conf. Robot. Autom. Eng. (ICRAE)*, Nov. 2020, pp. 126–130.
[36] R. Muntashir and L. Nurahmi, "Reconfiguration of cable driven parallel robot based on mobile base position," in *Proc. IEEE Int. Conf. Mechatronics Autom. (ICMA)*, Aug. 2022, pp. 563–568.
[37] S. Jiang, W. Song, Z. Zhou, and S. Sun, "Stability analysis of the food delivery robot with suspension damping structure," *Heliyon*, vol. 8, no. 12, Dec. 2022, Art. no. e12127.
[38] P. Xiong, A. Song, P. Ji, and X. Huang, "Study on ability of a mobile tracked robot for stair-climbing based on static analysis," in *Proc. IEEE Int. Conf. Cyber Technol. Autom., Control, Intell. Syst. (CYBER)*, Jun. 2015, pp. 1327–1332.
[39] C. Zhang, X. Jiang, M. Teng, and J. Teng, "Research on gait planning and static stability of hexapod walking robot," in *Proc. 8th Int. Symp. Comput. Intell. Design (ISCID)*, vol. 2, Dec. 2015, pp. 176–179.
[40] X. Gao, D. Cui, W. Guo, Y. Mu, and B. Li, "Dynamics and stability analysis on stairs climbing of wheel–track mobile robot," *Int. J. Adv. Robot. Syst.*, vol. 14, no. 4, 2017, Art. no. 1729881417720783.
[41] T. H. Lim, Y. S. Kim, J. H. Choi, H. S. Lee, and S. Y. Yang, "Development of tipping-over rate computation system for hydraulic excavator having crane function," in *Proc. 8th Russian-Korean Int. Symp. Sci. Technol.*, 2004, pp. 76–79.
[42] Y. Jia, X. Luo, B. Han, G. Liang, J. Zhao, and Y. Zhao, "Stability criterion for dynamic gaits of quadruped robot," *Appl. Sci.*, vol. 8, no. 12, p. 2381, Nov. 2018.
[43] P. Sardain and G. Bessonnet, "Forces acting on a biped robot. Center of pressure—Zero moment point," *IEEE Trans. Syst., Man, Cybern., A, Syst. Hum.*, vol. 34, no. 5, pp. 630–637, Sep. 2004.
[44] J. Pusey, A. Fattah, S. Agrawal, and E. Messina, "Design and workspace analysis of a 6–6 cable-suspended parallel robot," *Mechanism Mach. Theory*, vol. 39, no. 7, pp. 761–778, 2004.

HOR TAN received the master's degree from the Institut Teknologi Sepuluh Nopember (ITS), Indonesia, in 2021. Currently, he is a Lecturer with the National Polytechnic Institute of Cambodia. His research interests include the mathematical and mechanical design of mobile robots and kinematics of the cable-driven robots. His lecture background is related to mathematics and applies to mechanical software, such as noise and vibration, modern control engineering, and vehicle dynamics.

RIZAL MUNTASHIR received the master's degree from the Sepuluh Nopember Institute of Technology. Since 2021, he has been actively engaged in researches focused on mobile robots and cable-driven parallel robots. Currently, he is a Submarine Cable Engineer with Walsin Energy Cable System Company Ltd., Taiwan. He is a Responsible Engineer for the wire drawing and stranding processes.

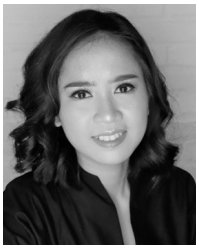

LATIFAH NURAHMI (Member, IEEE) received the Ph.D. degree in mechanical engineering from École Centrale de Nantes, France, in 2015. She is currently an Assistant Professor and the Head of the System and Control Engineering Laboratory, Department of Mechanical Engineering, Institut Teknologi Sepuluh Nopember, Surabaya, Indonesia. Her works have been published mainly in Elsevier and *ASME Transactions*. Her research interests include mechanism kinematics-dynamics, reconfigurable parallel mechanisms, and cable-driven parallel robots. She was awarded the L'Oréal-UNESCO for Women in Science National Fellowship 2020, Indonesia. Her Ph.D. thesis also won the third prize of Ma thèse en 180 secondes by the French Embassy and the Indonesian Ministry of Higher Education. She received the Best Paper from the IEEE IFToMM 5th International Conference on Reconfigurable Mechanisms and Robotics, in 2021, and she was a Grantee of the IFToMM Young Delegate Program 2018 to join as an Invited Speaker of the 5th IFToMM Asian Mechanism and Machine Science, which she also won the Best Interactive Poster. She won the Best Paper Award from the IEEE-IFToMM 5th International Conference on Reconfigurable Mechanisms and Robotics 2021. She received the National Award Pancasila National Icon of Science and Innovation 2023 from the Pancasila Ideology Development Agency, Indonesia. She is actively contributing as the Chair and a Reviewer of IFToMM and ASME conferences and journals.

BAMBANG PRAMUJATI (Member, IEEE) received the master's degree from the Department of Mechanical Engineering, University of Birmingham, U.K., in 1997, and the Ph.D. degree from the University of New Brunswick, Canada, in 2004. He is currently an Associate Professor with the Department of Mechanical Engineering, Institut Teknologi Sepuluh Nopember, Indonesia. He has received various national and international grants for his research works and community development programs. He is also actively involved in various industrial projects and research. In addition, he has received funding for academic and management-related training in the country and overseas. He works in several research areas, including industrial automation, control systems, model-based predictive control, and its application in manufacturing processes. He was a reviewer of various national research and scholarship grant selections. Up to now, he has served in various management positions in his institution. He is appointed as the vice-rector for research, innovation, partnership, and alumni.

ARI KURNIAWAN received the master's degree from the Institut Teknologi Bandung (ITB), Indonesia. He is currently pursuing the Ph.D. degree with the Department of IT Convergence Engineering, Kumoh National Institute of Technology, South Korea. He is a Lecturer with the Institut Teknologi Sepuluh Nopember (ITS), Surabaya, Indonesia. His research interests include automation and wearable devices for health monitoring.

UNGGUL WASIWITONO (Member, IEEE) received the master's degree from Monash University, Australia, in 2007, and the Ph.D. degree from Hiroshima University, Japan, in 2011. He is currently an Associate Professor with the Department of Mechanical Engineering, Institut Teknologi Sepuluh Nopember (ITS), Indonesia. His research interests include modeling and control of mechanical systems, anti-windup control, and robust control for underactuated mechanical systems.

STÉPHANE CARO (Member, IEEE) received the Engineering and M.Sc. degrees in mechanical engineering from École Centrale de Nantes, Nantes, France, in 2001, and the Ph.D. degree in mechanical engineering from the University of Nantes, in 2004.

He was a Post-Doctoral Fellow with the Centre for Intelligent Machines, McGill University, Montreal, QC, Canada, from 2005 to 2006. He is currently the Director of Research of the National Centre for Scientific Research (CNRS), Laboratory of Digital Sciences of Nantes (LS2N), UMR CNRS 6004, France. He is the Head of the Robots and Machines for Manufacturing, Society and Services (RoMaS) Team, LS2N. He is also a part-time Researcher with IRT Jules Verne, a mutualized industrial research institute. Moreover, he is a Lecturer with École Centrale de Nantes. He is the author of 90 articles published in international journals, 193 papers presented at international conferences, 59 contributions to books, and ten patents. His research focuses on the design, modeling, and control of cable-driven parallel robots and reconfigurable parallel robots.

Dr. Caro is a member of ASME and the IFToMM Computational Kinematics and ASME Mechanisms and Robotics Technical Committees. He was awarded the Accreditation to Supervise Research (HDR), in 2014. He is one of the two recipients of the 2018 Reviewers of the Year for *ASME Journal of Mechanisms and Robotics*. He is one of the two recipients of the 2019 Crossley Award, Mechanism and Machine Theory. He is ranked in Stanford's 2023 list of the 2% most cited scientists in their discipline. He is an Associate Editor of *ASME Journal of Mechanisms and Robotics*, IEEE Robotics and Automation Letters, and *The International Journal of Robotics Research*.